

Systematic Metastable Atmospheric Regime Identification in an AGCM

Christian Franzke¹, Illia Horenko², Andrew J. Majda³ and Rupert Klein²

¹British Antarctic Survey, Natural Environment Research Council, Cambridge, UK

²Institut für Mathematik, Freie Universität Berlin, Berlin, Germany

³Department of Mathematics and Climate, Atmosphere, Ocean Science, Courant Institute
of Mathematical Sciences, New York University, New York, NY, USA

November 28, 2008

Corresponding author address: Dr. Christian Franzke, British Antarctic Survey, High

Cross, Madingley Road, Cambridge CB3 0ET, UK, E-mail: chan1@bas.ac.uk

Abstract

In this study we apply a recently developed clustering method for the systematic identification of metastable atmospheric regimes in high-dimensional data sets generated by atmospheric models. The novelty of this approach is that it decomposes the phase space in, possibly, over-lapping clusters and simultaneously estimates the most likely switching sequence amongst the clusters. The parameters of the clustering and switching are estimated by a Finite Element approach. The switching amongst the clusters can be described by a Markov transition matrix. Possible metastable regime behavior is assessed by inspecting the eigenspectrum of the associated transition probability matrix.

Here we apply the recently introduced metastable data-analysis method to high-dimensional data sets produced by a barotropic model and a comprehensive atmospheric General Circulation Model (GCM). We are able to successfully identify significant and dynamically relevant metastable regimes in both models. The metastable regimes in the barotropic model correspond to blocked and zonal states. Similar regime states were already previously identified in highly reduced phase spaces of just one- and two-dimensions in the same model.

Next the clustering method is applied to a comprehensive atmospheric GCM where 7 significant flow regimes are identified. The spatial structures of the regimes correspond amongst others to both phases of the Northern Annular Mode and Pacific blocking. The regimes are maintained predominantly by transient eddy fluxes of low-pass filtered anomalies. It is demonstrated how the dynamical description of the slow process switching between the regimes can be acquired from the analysis results and an investigation of the resulting simplified dynamical model with respect to predictability is performed.

A predictability study shows that a simple Markov model is able to predict the regimes up to 6 days ahead, which is comparable to the ability of high resolution state-of-the-art numerical weather prediction models to accurately predict the onset and decay of blockings. The implications of our results for the derivation of reduced models for extended-range predictability are discussed.

1 Introduction

The last couple of decades have seen a continuing search for preferred and recurrent atmospheric flow patterns or regimes. Synopticians were the first to notice the existence of recurring atmospheric flow patterns, with the blocking phenomenon the most pronounced example (Baur 1951; Rex 1950). The existence of atmospheric regimes offers the potential of skillful extended-range predictions. In extended-range predictions one is not necessarily interested in forecasting the precise location of a cyclone on a particular day, rather one wants to forecast the overall weather situation for relatively long periods of time which are likely determined by regimes. For example, in a blocking situation the normal east-west propagation of migratory cyclones and anti-cyclones is obstructed by a quasi-stationary anticyclone so that they are forced on either a more north- or southward path. Since blockings can last for about a week or longer this will certainly influence regional weather over periods longer than the typical life span of synoptic-scale cyclones. Current numerical weather forecasting models used by operational centers have problems in accurately predicting the onset and decay of blockings (Tibaldi and Molteni 1990; Pelly and Hoskins 2003; Palmer et al. 2008). While the high-resolution ensemble prediction system of European Centre for Medium-Range Weather Forecasts (ECMWF) can predict Euro-Atlantic block onsets up to 6 days and block decay up to 10 days in advance its limits in the central Pacific region for block onset and decay are 4 and 8 days and 4 and 6 days in the west Pacific region (Pelly and Hoskins 2003). Thus, there is a strong need to understand better the dynamical origins of regimes and predict their onset and decay. Of special interest are low-order models with predictive skill in forecasting the onset and decay of regime states like blocking because such models are computationally much cheaper than numerical weather prediction models.

In a pioneering study Charney and DeVore (1979) tried to explain the origin of flow regimes in dynamical terms. They used a highly truncated barotropic model for flow over topography and found two stable fixed point solutions. One corresponds to a zonal flow configuration and the other to a blocking situation. Similar results have been found by Wiin-Nielsen (1979), Charney and Straus (1980) and Legras and Ghil (1985). On the other hand, studies by Reinhold and Pierrehumbert (1982), Tung and Rosenthal (1985) and Majda et al. (2006) find that the distinct flow regimes are not close to the fixed points of the planetary waves.

While the above studies try to explain regime behavior in dynamical terms, there is also a huge body of work whose main focus is on the statistical identification of recurring and/or persistent flow patterns in datasets from either models or reanalysis data sets. The methods of choice include cluster analysis (Mo and Ghil 1988; Cheng and Wallace 1993; Michelangeli et al. 1995; Smyth et al. 1999), nonlinear principal component analysis (Monahan et al. 2000) and looking for quasi-stationary patterns (Vautard 1990). Michelangeli et al. (1995) find that recurrent patterns identified by cluster analysis do not necessarily correspond to persistent (quasi-steady) flow regimes.

The search of deviations from Gaussianity and especially multiple extrema in the phase space of the leading Empirical Orthogonal Functions (EOF) or Planetary waves is another way of identifying flow regimes (Hansen and Sutera 1986; Kimoto and Ghil 1993; Corti et al. 1999; Monahan et al. 2000; Christiansen 2005; Berner and Branstator 2007). In this regime view, deviations from Gaussianity are the imprint of preferred and/or recurrent flow patterns due to nonlinear dynamics. Thus, the Gaussian part of the PDF is thought of consisting of only noise and/or linear dynamics which cannot create regime behavior. The statistical significance and existence of multiple extrema

in the PDFs of observed data is a topic of debate in the recent literature (Nitsche et al. 1994; Stephenson et al. 2004; Ambaum 2008). Furthermore, recent studies reveal that the PDFs of the leading few EOFs of long integrations with a 3-level quasi-geostrophic model (Franzke and Majda 2006) and an atmospheric GCM (Berner and Branstator 2007) exhibit only slight although significant deviations from Gaussianity. But these PDFs are, nonetheless, unimodal to first order. The deviations from Gaussianity take the form of some weak skewness and ridges with enhanced density in the case of joint PDFs (Berner and Branstator 2007; Franzke et al. 2005, 2007; Franzke and Majda 2006).

Recent studies introduced the concept of metastability for the identification of flow regimes (Majda et al. 2006; Franzke et al. 2008; Horenko et al. 2008a, 2008b). In these studies a Hidden Markov Model (HMM) is fitted to geophysical circulation model or reanalysis data. A Hidden Markov Model is designed to describe the situation in which part of the information of the system is unknown or hidden and another part is observed. In this context the 'observed' variable can be a representative variable of low-frequency variability whose dynamics may depend crucially on the overall flow configuration (e.g. zonal or blocked flow), which is unknown. The behavior of this latter, "hidden" variable is described by a Markov transition matrix. If the eigenvalue spectrum of the Markov transition matrix exhibits a gap then the corresponding hidden states can be associated with flow regimes. Thus, this method uses both geometrical information of clustering in the phase space and temporal information of the hidden state evolution simultaneously. This is a major advantage over most methods described above. The HMM approach focuses on the persistence rather the recurrence property of regimes and can also identify regimes in nearly Gaussian or unimodal data.

Once atmospheric regimes have been found it is important to examine the skill in predicting the onset, decay and transitions of the regime states. A simple approach for such forecast experiments is to fit a Markov chain to the data (e.g. Crommelin 2004; Deloncle et al. 2007, Kondrashov et al. 2008). In the HMM framework the Markov transition matrix of the regime transitions is already part of the regime identification algorithm (Majda et al. 2006; Horenko et al. 2008b; Franzke et al. 2008) and all data points get systematically assigned to a cluster due to the determination of the most likely hidden state sequence. Such approaches show useful forecasting skill.

In this study we apply a recently developed method (Horenko 2008b, 2008c) which is especially suited for the investigation of high-dimensional data sets. This method allows for identification of hidden metastable regimes based on the differences in *local* EOF characteristics for each of the regimes, i. e., it allows simultaneous regime identification and dimension reduction for time series of very high dimensionality. Major advantage of the method, compared to the available HMM-based approaches described in the context of meteorological applications (Majda et al. 2006, Franzke et al. 2008; Horenko 2008b, Horenko 2008c), is its independence of *a priori* assumptions about the probability models (like Markov- and Gauss- assumptions in context of HMM-Gauss method). In the present paper we demonstrate how such assumptions can be verified *a posteriori* for realistic applications and how the *optimal* number of the *hidden* regimes can be identified, resulting in construction of reduced predictive Markovian models. The method and the concept of metastable regimes are described in section 2. In section 3 we test the method on the well studied barotropic flow over topography and in section 4 we apply the method to a comprehensive atmospheric GCM and give conclusions in section 5.

2 Finite Element Clustering and Metastability

In this section we introduce the Finite Element Clustering method and the concept of metastable regimes.

Finite Element Clustering

For the identification of regime states in high-dimensional geophysical data sets we are utilizing the recently developed Finite Element Clustering (FEC) method (Horenko 2008b, 2008c). This method relaxes the restriction of the recently used HMM based methods (Majda et al. 2006, Franzke et al. 2008 and Horenko et al. 2008b) where the hidden transition process has to be a Markov process and of the conditional independence relation, Gaussianity and low-dimensionality of the observed data. This is a major improvement over the HMM method since geophysical data are not necessarily Markovian and locally Gaussian.

The used method simultaneously estimates the clusters (corresponding to regimes) and the most likely hidden state transitions between the clusters. In this clustering approach we assume that the dynamical system consists of two variables: one variable Y which can directly be observed but this observed variable depends on a 'hidden' variable X (also referred to as cluster) which cannot be directly observed. In the present context the 'hidden' variable is associated with flow regimes which strongly influence the observed variable.

Here we use the clustering approach FEM-K-EOFs recently developed by Horenko (2008a). This method is based on the minimization of the averaged clustering functional of a given time series $\mathbf{x}(t)$. The FEC method then tries to characterize the time series by K clusters (or hidden states) and the most likely cluster sequence $\gamma_i(t)$, where the index i indicates the i -th cluster and

$\gamma_i(t)$ denotes the probability that the state of the system at time t belongs to cluster i . Thus, for a *a priori* given number K of clusters the FEC method tries to minimize the distance of the actual trajectory (in an appropriate metric) to one of the K clusters at time t . This means, that we are looking simultaneously for the cluster locations and the time evolution of the system in the space spanned by the clusters.

This method considers the clustering of possibly non-stationary multidimensional data $x_t \in \mathbf{R}^d$ as a minimization problem

$$\mathbf{L}(\Theta, \Gamma) = \sum_{i=1}^K \gamma_i(t) g(x(t), \theta_i) \rightarrow \min_{\Gamma(t), \Theta} \quad (1)$$

subject to constraints

$$\sum_{i=1}^K \gamma_i(t) = 1, \forall t \in [0, T] \quad (2a)$$

$$\gamma_i(t) \geq 0, \forall t \in [0, T], i = 1, \dots, K. \quad (2b)$$

where we want to minimize the object \mathbf{L} . The object $\gamma_i(t)$ can be interpreted as the probability that the system at time t belongs to the i -th cluster and θ_i denotes the parameters and location of the i -th cluster. The corresponding cluster distance functional characterizes the quality of describing given observation x_t at time t by a certain model i with parameters θ_i (see Horenko 2008a for more details). As it was demonstrated in Horenko (2008a), one can incorporate additional information into the optimization like some smoothness assumptions in space of functions ($\Gamma(\cdot)$) and then apply a finite Galerkin time-discretization of this infinite-dimensional Hilbert space. For example, one can impose the weak differentiability of functions γ_i , i. e.:

$$|\gamma_i|_{\mathcal{H}^1(0,T)} = \|\partial_t \gamma_i(\cdot)\|_{\mathcal{L}_2(0,T)} = \int_0^T (\partial_t \gamma_i(t))^2 dt \leq C_\epsilon^i < +\infty, \quad i = 1, \dots, \mathbf{K}. \quad (3)$$

For a given observation time series, the above constraint limits the total number of transitions between the clusters and is connected to the metastability of the hidden process $\Gamma(t)$ (Horenko 2008b).

The minimization functional now takes the form

$$\mathbf{L}^\epsilon(\Theta, \Gamma, \epsilon^2) = \mathbf{L}(\Theta, \Gamma) + \epsilon^2 \sum_{i=1}^{\mathbf{K}} \int_0^T (\partial_t \gamma_i(t))^2 dt \rightarrow \min_{\Gamma, \Theta}. \quad (4)$$

where ϵ^2 is a Lagrange-multiplier, $\Gamma(t) = (\gamma_1(t), \dots, \gamma_K(t))$ denotes a vector of cluster weights and $\Theta = (\theta_1, \dots, \theta_K)$ the corresponding orthogonal projectors $\theta_i = \mathbf{T}_i \in \mathbf{R}^{n \times m}$ and the model distance function is given by $g = |x(t) - \mathbf{T}_i^T \mathbf{T}_i x(t)|^2$ where \mathbf{T}_i is a $n \times m$ dimensional orthogonal projection matrix ($m \ll n$), where n is the dimension of the state vector x and m is the dimension of the EOF manifold used for the projection. The optimization problem is now solved by a Finite Element approach (see Horenko 2008b, 2008c for more information and a detailed description of the algorithm).

Metastable Regimes and model reduction:

The studies by Majda et al. (2006), Franzke et al. (2008) and Horenko et al. (2008b) introduced the concept of metastable atmospheric flow regimes. Here we want to briefly review this concept. In this study we refer to metastable regimes if the eigenvalue spectrum of the Markov transition matrix, describing the switching between the clusters, has a statistically significant gap. Such a gap indicates that the state space S of X can be decomposed in two or more sets with relatively infrequent transitions between those sets; thus, the Markov chain is said to be metastable (see Majda et al. 2006, Franzke et al. 2008 and Horenko et al. 2008b for more details) and the reduced Markov chain describes only the effective, slow transitions between metastable sets. The aim of this study is to identify the states where the system stays for long times before it eventually makes

a transition to another regime state. Thus, here we look only for a small set of cluster states which have only infrequent transitions amongst them.

The concept of model reduction is best described by an example. As an example we take the 4×4 transition matrix from Franzke et al. (2008):

$$A = \begin{pmatrix} 0.49 & 0.47 & 0.03 & 0.01 \\ 0.47 & 0.49 & 0.01 & 0.03 \\ 0.02 & 0.01 & 0.53 & 0.44 \\ 0.01 & 0.01 & 0.44 & 0.54 \end{pmatrix} \quad (5)$$

which has the eigenvalues $\lambda_1(A) = 1.0$, $\lambda_2(A) = 0.935$, $\lambda_3(A) = 0.096$ and $\lambda_4(A) = 0.018$. The slow dynamics (or low-frequency behavior) of this Markov chain can be approximated by a 2×2 transition matrix, by lumping together each of the two sub-matrices $\{1,2\}$ and $\{3,4\}$. The lumping together is done in this example by summing over the elements A_{11} , A_{12} , A_{21} and A_{22} and dividing by 2 to give the element \tilde{A}_{11} and by summing over A_{13} , A_{14} , A_{23} and A_{24} and dividing by 2 to give the element \tilde{A}_{12} and so on for the sub-matrix $\{3,4\}$. By doing so we get the reduced matrix

$$\tilde{A} = \begin{pmatrix} 0.96 & 0.04 \\ 0.025 & 0.975 \end{pmatrix}, \quad (6)$$

which has the same leading eigenvalue structure, $\lambda_1(\tilde{A}) = 1.0$ and $\lambda_2(\tilde{A}) = 0.935$, as the original transition matrix A . The transition matrix \tilde{A} has, therefore, the same low-frequency behavior as A . This reduction is important in the present context, because we won't know the exact number of regimes in atmospheric data sets a priori (if they exist at all). Thus, the examination of the eigenvalue spectrum provides an objective means to identify the number of regime states. The lumping together of sub-matrices can be easily done for rather low-dimensional transition matrices

but is almost impossible for high dimensional matrices. For such matrices with large dimension we have to inspect the eigenvalue spectrum in order to derive a lower dimensional transition matrix. In case that the eigenvalue spectrum exhibits a gap, we can utilize the number of eigenvalues above the gap, those close to 1. This number constitutes then the number of states for a new estimation of the transition matrix.

2.1 Metastability, Markovianity and Embedding of Hidden State Sequence

In this study we want to quantify metastability by looking for the existence of a significant gap in the eigenvalue spectrum of a Markov transition matrix of the hidden state sequence. We have to be careful when inspecting the hidden state sequence $\Gamma(t)$ identified by the FEC method because it is not necessarily Markovian. This is partly due to the state space reduction of the full dynamics to only a few hidden states (clusters). In order to examine if the hidden state sequence is Markovian and to fit a Markov transition matrix we use the recently developed method for estimation of a Markov transition matrix by fitting a generator to the hidden state sequence (Metzner et al. 2007). In case we are unable to fit a generator this means the hidden state sequence is not Markovian. In order to make the hidden state sequence Markovian we choose to embed the hidden state sequence time series (Broomhead and King 1986; Horenko 2008b). In order to embed, we take the one-dimensional hidden state sequence $\Gamma(t)$ and create a two-dimensional time series

$$\tilde{\Gamma}(t+1) = \begin{pmatrix} \Gamma(t) \\ \Gamma(t+1) \end{pmatrix}, \tilde{\Gamma}(t+2) = \begin{pmatrix} \Gamma(t+1) \\ \Gamma(t+2) \end{pmatrix}, \tilde{\Gamma}(t+3) = \begin{pmatrix} \Gamma(t+2) \\ \Gamma(t+3) \end{pmatrix}, \dots \quad (7)$$

We now repeat the generator estimation with this new time series. If this time series is still not Markovian we increase the embedding dimension

$$\tilde{\Gamma}(t+2) = \begin{pmatrix} \Gamma(t) \\ \Gamma(t+1) \\ \Gamma(t+2) \end{pmatrix}, \dots \quad (8)$$

and so on until the embedded time series $\tilde{\Gamma}$ is Markovian and we can successfully fit a generator. If the analyzed time-discrete process $\Gamma(t)$ has a finite memory depth d , the procedure described above will need $d - 1$ iterations to construct a Markov process (see Horenko 2008b). Note, that by doing so we built in the Markov assumption of the hidden state sequence *a posteriori* and do not need to make *a priori* any assumption regarding Markovianity and conditional independence of the observed time series. This is a major advantage over the previous approaches based on HMM (Majda et al. 2006; Horenko et al. 2008b; Franzke et al. 2008).

If the Markov hypothesis is justified, the Markov transition probability matrix

$$P_{ij} = \mathbb{P} \left[\tilde{\Gamma}(t) = s_j | \tilde{\Gamma}(t-1) = s_i \right], \quad (9)$$

can be estimated, describing the probabilities of transitions between different identified regimes $s_1, \dots, s_{\mathbf{N}}$ (where \mathbf{N} is the total number of distinct regime sequences resulting from the embedding procedure). Note that the total number of non-zero transition matrix elements scales polynomially with respect to embedding dimension, this sets a natural upper limit of the embedding dimension for a time series $\Gamma(t)$ of the fixed given length (since with growing number of transition matrix parameters the estimation problem can become ill-posed, see Horenko 2008d). As follows from the maximum log-likelihood principle, the optimal values of the transition probability matrix can be

estimated directly from the time series $\tilde{\Gamma}(t)$:

$$P_{ij} = \frac{N_{ij}}{\sum_{k=1}^{\mathbf{N}} N_{ik}}, \quad (10)$$

where N_{ij} is the number of observed direct transitions between the states s_i and s_j along the analyzed series and $\sum_{k=1}^{\mathbf{N}} N_{ik} \neq 0$ (see Horenko 2008d). If we define a discrete probability density function for the observed Markovian process $\tilde{\Gamma}(t)$ as $\pi(t) = (\pi_1(t), \dots, \pi_{\mathbf{N}}(t))$ (where $\pi_k(t) = \mathbb{P}[\Gamma(t) = s_k]$), then the temporal evolution of this quantity can be described with the following *deterministic equation*:

$$\pi(t_0 + \tau) = \pi(t_0)P^\tau, \quad (11)$$

where τ is some positive integer, e.g., a number of days. If the matrix P is estimated from the given embedded data Γ according to (10), then defining

$$\pi_k(t_0 + \tau) = \begin{cases} 1 & s_k = \Gamma(t_0), \\ 0 & \text{otherwise.} \end{cases}, \quad (12)$$

one can calculate the *prediction* as a Markovian probability distribution at some later time $t_0 + \tau$ from (11). In the following, we will demonstrate the application of this procedure in context of atmospherical regime predictions.

3 Topographic Stress Model

The ideal barotropic quasi-geostrophic equations with a large scale zonal mean flow U on a $2\pi \times 2\pi$ periodic domain (e.g. Carnevale and Frederiksen, 1987; Grote et al. 1999; Majda et al. 1999, 2003,

2006, 2008; Franzke et al. 2008) are given by

$$\begin{aligned}\frac{\partial q}{\partial t} + \nabla^\perp \psi \cdot \nabla q + U \frac{\partial q}{\partial x} + \beta \frac{\partial \psi}{\partial x} &= 0 \\ q &= \Delta \psi + h \\ \frac{dU}{dt} &= \frac{1}{4\pi^2} \int h \frac{\partial \psi}{\partial x} dx dy\end{aligned}\tag{13}$$

with q the potential vorticity, U the large scale zonal mean flow, ψ the stream function, and h the topography. In (13), the mean flow changes in time through the topographic stress; this effect is the direct analog for periodic geometry of the change in time of angular momentum due to mountain torque in spherical geometry.

The metastable regime characteristics have been already described extensively in Majda et al. (2006) and Franzke et al. (2008) based on the analysis of a reduced phase space of just one- and two-dimensions. Here we utilize this model to briefly compare the FEC method in the full phase space with the previously used HMM method in a highly reduced phase space. For this purpose the whole data set consisting of 57 Fourier modes and the large-scale mean flow U is used. The length of the time series is 50000 time units sampled every quarter time unit.

An examination of the hidden state sequence reveals that this sequence becomes Markovian for an embedding dimension of 5 (which corresponds to 1.25 time units). The eigenvalue analysis for the corresponding transition matrix reveals three metastable states (Fig. 1). There is a second gap after the fifth eigenvalue, though it is smaller than the gap after the third eigenvalue. Since together with the eigenvalues we also display the 95% significance levels based on the sampling of probability matrix distributions (Noe 2008). This shows that the leading eigenvalues are very accurately estimated and that the gap is significant.

The corresponding flow patterns correspond to two zonal flow patterns with different magnitudes and one retrograde (blocking-like) pattern (not shown) which are very similar to the patterns in Franzke et al. (2008). Thus, this result is consistent with the HMM analysis of Majda et al. (2006) and Franzke et al. (2008) where they only analysed one-dimensional or two-dimensional time series consisting of the large scale mean flow U and the first Rossby wave mode. This confirms that in this model the regime dynamic is encoded in the large scale mean flow U and the first Rossby wave mode and, furthermore, shows the ability of the FEC approach of identifying dynamically relevant metastable regimes in high-dimensional data sets of geophysical flow models.

4 Regimes in an atmospheric GCM

Now we apply the FEC method to the comprehensive National Center of Atmospheric Research (NCAR) GCM CCM0. This model is based on the primitive equations with a full physical parameterization package for processes like radiation and convection. It has 9 vertical levels and its horizontal truncation is rhomboidal 15. The model has been used recently by Berner and Branstator (2007) and Branstator and Berner (2005). Franzke et al. (2008) have used the same model for a HMM based regime analysis. Though this model cannot be considered to be state-of-the-art, it still has a very realistic representation of low-frequency variability and planetary wave dynamics which are the main focus of our study.

The data set we are using stems from a realization of a perpetual January integration of CCM0 with fixed solar insolation for January and constant Sea Surface Temperature (SST) and has a length of 50000 days with samples stored every 12 hours. To arrive at a reduced system the AGCM

states are represented in terms of 500 hPa geopotential height EOFs (in a standard squared metric). The spatial pattern of the first EOF (Fig. 2a) bears similarity with the Northern Annular Mode (NAM; Thompson and Wallace 1998) and the second EOF pattern (Fig. 2b) is somewhat similar to the Pacific-North American (PNA) pattern, even though its Pacific center is phase shifted to the west. The other leading patterns are not similar to any well known teleconnection patterns; they mainly represent wave trains around the Arctic (Fig. 2c and d). The explained variances of the EOFs do not show any gap; the explained variance decays rather monotone as is typical for such data sets (Fig. 3a). The first 100 EOFs explain about 97.5% of the total variance (Fig. 3b). Thus, we will first focus on this subset for the metastability analysis with the FEC method. As we will see below this 100 dimensional subspace is more than sufficient to capture the essential metastable dynamics of CCM0.

4.1 Eigenvalue Spectrum

The FEC algorithm (Horenko 2008b, 2008c) is used to identify hidden states in the subset of the first 100 EOFs of 500 hPa geopotential height. An examination of the hidden state sequence reveals again that the sequence becomes Markovian for an embedding dimension of 5 (which corresponds to 2.5 days). Next a Markov transition matrix is fitted to this hidden state sequence. The eigenvalue spectrum of the Markov transition matrix is displayed in Fig. 4 and reveals a gap after the 7th eigenvalue. In Fig. 4 are also displayed the 95% significance levels of the eigenvalue estimates based on the sampling of the Markovian transition probability matrices (Noe 2008). This shows that the first 7 eigenvalues are estimated very accurately, whereas, higher eigenvalues contain substantial uncertainty. Hence, the eigenvalue gap is significant.

Furthermore, all eigenvalues are real. Thus, the corresponding flow patterns of the hidden states correspond to standing planetary Rossby waves and not to travelling Rossby waves. In order that the hidden states would correspond to travelling Rossby waves some of the eigenvalues would need to have imaginary components. The fact that the hidden states correspond to standing waves indicates that they are persistent and quasi-stationary flow regimes. That the spatial structures of the hidden states in CCM0 resemble well known pattern found in reanalysis data will be shown below.

Furthermore, we examined the Markov transition matrix also for preferred transitions between the hidden states. For this purpose we estimate the transition matrix which describes the switching between the hidden states. For this purpose we count only the transitions to a different hidden state. By doing so we get the following transition matrix:

$$A = \begin{pmatrix} 0 & 0.11 & \mathbf{0.52} & 0.13 & 0 & 0 & 0.23 \\ 0.04 & 0 & \mathbf{0.23} & 0.12 & 0.16 & \mathbf{0.33} & 0.12 \\ \mathbf{0.23} & 0.19 & 0 & \mathbf{0.22} & 0 & 0.17 & 0.18 \\ 0.13 & 0.19 & 0.09 & 0 & \mathbf{0.26} & 0.07 & \mathbf{0.24} \\ 0 & 0.20 & 0 & \mathbf{0.24} & 0 & \mathbf{0.33} & 0.21 \\ 0 & 0.18 & 0.18 & 0.13 & \mathbf{0.35} & 0 & 0.13 \\ 0.06 & 0.11 & \mathbf{0.24} & \mathbf{0.23} & 0.13 & 0.21 & 0 \end{pmatrix} \quad (14)$$

All transition probabilities in above matrix are considered to belong to a preferred transition if their probability is significant larger than when all transitions would be equally likely. In order to find the preferred transitions we also estimate significance intervals for the transition probabilities according to Horenko et al. (2008a). All matrix elements in bold are significant at the 99.9%

level and, thus, describe preferred transitions. As can be seen, each hidden state has at least one preferred transition to another state, while states 2, 3, 4, 5 and 7 have two preferred transitions to other states. These preferred transitions offer the possibility of skillful predictions, which will be investigated below.

4.2 Hidden State Composites

The following discussion is based on composite fields based on the hidden state path. For example, to compute the composite of the conditional mean field of geopotential height of hidden state 1, we average the geopotential height fields over all times when the hidden state sequence belongs to hidden state 1 and so forth. A representative sequence of the hidden state path is displayed in Fig. 5. The conditional mean states corresponding to the hidden states sequence based on 7 hidden states are displayed in Fig. 6. Hidden states 1 and 3 resemble the negative phase of the NAM and hidden states 5 and 6 the positive NAM phase. Hidden state 4 bears some resemblance with the PNA whereas hidden states 2 and 7 are wave trains extending over the Pacific and Atlantic oceans; both hidden states also bear some similarity with EOF3 and EOF4 respectively. The fact that hidden states 1 and 3 and also 5 and 6 have striking similarities does not indicate that those flow fields are just different phases of a travelling planetary wave. For this to be the case the eigenvalue spectrum would need to contain complex eigenvalues. The hidden states 3 and 5 are also similar to the anomalous states identified by Branstator and Berner (2005) and Berner and Branstator (2007).

The projection of the hidden states onto the EOFs (Fig. 7a) shows that they mainly project on the leading 5 EOFs. Also the pattern correlation between the hidden state composites and the

EOFs reveals the dominance of the first 5 EOFs for the hidden states (Fig. 7b). This suggests that a 5 dimensional subspace is sufficient to capture the essential metastable behavior. The persistence characteristics show that hidden state 1 is much more persistent than the other 6 hidden states (Figs. 8). The second most persistent hidden state is hidden state 5 which projects strongly onto the positive NAM.

Another way to look at the geographical structure of the hidden states is to investigate the left eigenvectors of the Markov transition matrix (Fig. 9). We derive the geographical structure of the left eigenvectors as a weighted mean of the hidden state composites according to the left eigenvector. Because the transition matrix is a stochastic matrix the first eigenvalue is associated with the invariant measure and, thus, corresponds to the climatological mean state (not shown). The second eigenvector has its main centers of action over the North Pacific and the west coast of Canada. Its positive anomaly over the Pacific corresponds to a blocking like situation. The remaining eigenvectors (3 through 7) project predominantly on both phases of the Northern Annular Mode and are dominated by their center of action over the Arctic. Eigenvectors 4 and 7 are also similar to the anomalous states corresponding to the means of two-component Gaussian mixtures in the study by Berner and Branstator (2007). Furthermore, eigenvectors 3 and 7 correspond to the anomalous states found at the dynamical center of a quasi-linear region in the phase space of the first 4 EOFs by Branstator and Berner (2005).

In order to explore some of the dynamical processes responsible for the regime behavior we examine composites of the transient eddy forcing ($-\nabla^{-2}\nabla \cdot (\mathbf{u}\zeta)$ where \mathbf{u} denotes the horizontal wind vector and ζ the relative vorticity; these are anomalies with respect to their climatological mean fields) conditional on the respective hidden state. These composites are displayed in Fig.

10 for the respective hidden states and give an indication of the nonlinear forcing involved in maintaining the respective hidden state mean fields. The geographical structure of the transient eddy forcing fields suggest that the transient eddy forcing over the North Pacific plays a major role in the regime dynamics. The transient eddy forcing is mainly concentrated over the Pacific ocean for hidden states 2 through 6 (Figs. 10b-f). The transient eddy forcing mainly acts over both the Pacific ocean and Asia for hidden state 1 (Fig. 10a) and over both the Pacific and Atlantic oceans for hidden state 7 (Fig. 10g). A comparison with the transient eddy forcing from low-pass filtered¹ (periods larger than 10 days; superscript L) anomalies ($-\nabla^{-2}\nabla\cdot(\mathbf{u}^L\zeta^L)$), high-pass filtered (periods less than 10 days; superscript H) anomalies ($-\nabla^{-2}\nabla\cdot(\mathbf{u}^H\zeta^H)$) and the interaction between high- and low-pass filtered anomalies ($-\nabla^{-2}\nabla\cdot(\mathbf{u}^H\zeta^L + \mathbf{u}^L\zeta^H)$) reveals a complex picture. While there is a preference of both the low- and high-pass filtered transient eddy fluxes to play a role in the more annular mode like regimes (Hidden states 1, 2 and 5; Fig. 10; note the smaller contour interval of the high-pass filtered transient eddy forcing) this is less the case for hidden state 6. Our analysis also reveals that the low-frequency transient eddy fluxes are dominant for the more wave train like hidden states 2 and 7 and also the PNA like regime state (Fig. 10: middle column). The interaction between high- and low-pass filtered anomalies (not shown) are of only secondary importance. Overall, the low-pass filtered transient eddy fluxes are involved in the maintenance of all regime states, while the high-frequency transient eddy fluxes are involved in only the annular mode like regimes states. The involvement of the low-pass filtered transient eddy fluxes offers the possibility of successful predictions of the regimes states which will be investigated next. It also has to be mentioned that the correspondence between the transient eddy fluxes (Fig. 10) and the

¹We use a digital Lanczos filter with 31 weights for the filtering

regime states (Fig. 6) is not perfect indicating that other processes, linear processes like vorticity advection, also contribute to the regime maintenance.

4.2.1 Predictability

The successful identification of metastable regimes offers the prospect of successful long-range prediction of at least the regime states while not necessarily the precise weather conditions at a particular day. In current weather and climate prediction models the skillful forecasting of the onset and decay of blocking situations is still a major problem (Tibaldi and Molteni 1990; D’Andrea et al. 1998; Pelly and Hoskins 2003; Palmer et al. 2008).

Since some of our metastable regime states are associated with blocking like situations this offers the possibility that it is at least possible to generate skillful probabilistic forecasts of the onset and decay of blockings or other regime states by predicting the evolution of the hidden states. To test the predictive skill of the Markov matrix in predicting the hidden state sequence we split our data set in half and use only the first half to estimate the Markov transition matrix of the hidden state and then utilize only the second half of the data set for forecast experiments. To calculate the Markovian prediction, we use the procedure based on (11) described above for different values of the embedding dimension. In Fig. 11 is displayed the percentage of successful predictions of the hidden state for two sets of experiments. One is based on the original hidden state sequence and the other uses an embedding of the hidden state sequence with embedding dimension 5. For this embedding the hidden state sequence becomes Markovian. Both settings show an almost exponential decay in prediction skill with an e-folding time-scale of about 6 days and the short-term predictability is enhanced for up to 6 days forecasts for the case with embedding. This offers the prospect of

making successful predictions of the onset and decay of blockings and other regime states of up to 6 days in advance. As is well known, current weather forecasting models have problems in accurately predicting the onset and decay of blockings. Thus, our empirical-dynamical Ansatz of predicting the hidden-state sequence is a promising Ansatz in improving prediction skill and might serve as a reference model in operational weather prediction.

5 Conclusions

In this study we applied the recently developed Finite Element Clustering method (Horenko 2008b, 2008c) in order to objectively identify metastable regimes in a high-dimensional data set produced by a comprehensive atmospheric GCM. This method is designed to identify hidden structures in high-dimensional data sets. We first applied this method to barotropic flow over topography where we confirmed earlier results on regime behavior with a HMM method in a reduced subspace. Next we applied the FEC method to a comprehensive GCM, the NCAR GCM CCM0. The FEC method is able to identify in a 100 dimensional phase space of 500 hPa geopotential height seven dynamically significant metastable regimes. Some of the regimes correspond to the positive and negative phase of the Northern Annular Mode, respectively. Others are very similar to the states which are at the centers of nonlinear features in the mean tendency fields in the study by Branstator and Berner (2005; see their Fig. 12). The existence of hidden states is also consistent with the results by Berner and Branstator (2007) who investigated the same GCM data set. In their study they also find evidence for the existence of two regimes when examining the phase space spanned by the first 4 EOFs (see their Fig. 16). These two regime states are very similar to some of our hidden states.

In a previous study by Franzke et al. (2008) no evidence of metastable regimes were found by investigating the same GCM data set using the HMM method. In their study only one-dimensional time series of the leading four EOFs were separately investigated by HMM. In the present study we examined a very high-dimensional phase space and with a more advanced method which relaxes some major assumptions of HMMs and simultaneously estimate the regime and dimension reduction. This shows that the regime behavior in CCM0 is only visible in a multi-dimensional phase space and not in projections on individual EOFs. Suggesting that in this GCM the regime behaviour is due to a nonlinear interactions of various EOFs and cannot be found by just examining individual EOFs separately.

One important question is which processes are responsible for maintaining the hidden states. Since this model is run in a perpetual January mode with fixed solar insolation and SST all possible regime behavior is due to nonlinear atmospheric dynamics alone. Our results suggest that the transient eddy forcing plays a major role in maintaining the regimes. Though the correspondence between the transient eddy forcing and the regime states is not perfect. This suggests that also other processes contribute to the maintenance of the regimes. Both low- and high-frequency eddies contribute to the transient eddy forcing with the low-frequency eddies playing the major role, though our results also show that the storm tracks have distinct differences between the hidden states. This suggests that mainly the nonlinear interaction amongst low-frequency planetary Rossby waves are involved in the regime dynamics of all hidden states while the high-frequency eddies contribute to the maintenance of the more annular mode like regimes. It is also noteworthy that most of the transient eddy forcing takes place over the Pacific ocean. This suggests that in CCM0 the Pacific region plays a major role for the regime dynamics. While this analysis offers some

insight into the relevant regime dynamics, the exact dynamical processes leading to the switching between the atmospheric regimes is still an open question and will be further addressed in future studies.

The very long persistence property of the regime state corresponding to the negative NAM phase offers the possibility of skillful extended-range predictions if one is able to successfully predict the onset and decay of the hidden states and the switching amongst the hidden states. This particular hidden state also corresponds to a blocked circulation in the sense that this hidden state leads to a weakening and/or meridional displacement of the jet stream. Such a distortion of the jet stream is usually associated with a blocked flow. If replacements of the jet stream on a hemispheric scale associated with the NAM leads to simultaneous blockings in the Pacific and Atlantic regions needs further study.

Our predictability study shows that a simple Markov model for the evolution of the hidden states has predictive skill for about 6 days in successfully predicting the hidden state. This is about the same skill as the ECMWF Ensemble Prediction System in T255 resolution has in predicting the onset and decay of blocking situations (Pelly and Hoskins 2003) but with a much lower computational cost. Thus, such a model could serve as a complementary model in operational ensemble weather prediction. These results have implications for the derivation of low-order models for skillful extended-range prediction. Such low-order models need to capture the essential dynamics responsible for the switching amongst the regime states. Thus, to predict this switching the low-order models need to accurately capture the leading eigenvalue structure of the Markov transition matrix which determines the evolution of the low-frequency modes and more importantly also the regime switching. The prediction prospects of such models has been already alluded to in

Majda et al. (2006) where it has been shown that a single stochastic differential equation is capable of capturing the metastable low-frequency regime behavior compared with the fully turbulent 57-mode topographic stress model. Horenko et al. (2008b) report skillful short-term predictions of temperature for Europe with a model that combines hidden Markov models and linear stochastic differential equations. Hence, our results show the potential for practical use of low-dimensional models for extended-range predictions.

Acknowledgments: We thank Dr. Grant Branstator and Andy Mai for providing us with the CCM0 data set.

References

- Ambaum, M. H., 2008: Unimodality of Wave Amplitude in the Northern Hemisphere. *J. Atmos. Sci.*, **65**, 1077–1086.
- Baur, F., 1951: Extended range weather forecasting. *Compendium of Meteorology*, American Meteorological Society, 814–833.
- Berner, J. and Branstator, G, 2007: Linear and Nonlinear Signatures in the Planetary Wave Dynamics of an AGCM: Probability Density Functions. *J. Atmos. Sci.*, **64**, 117–136.
- Branstator, G. and J. Berner, 2005: Linear and Nonlinear Signatures in the Planetary Wave Dynamics of an AGCM: Phase Space Tendencies. *J. Atmos. Sci.*, **62**, 1792–1811.
- Broomhead, D. S. and G. P. King, 1986: Extracting Qualitative Dynamics from Experimental Data. *Physica D*, **20**, 217–236.
- Carnevale, G. and J. S. Frederiksen, 1987: Nonlinear Stability and Statistical Mechanics for Flow over Topography. *J. Fluid Mech.*, **175**, 157–181.
- Charney, J. G., and J. G. DeVore, 1979: Multiple Flow Equilibria in the Atmosphere and Blocking. *J. Atmos. Sci.*, **36**, 1205–1216.
- Charney, J. G., and D. M. Straus, 1980: Form-Drag Instability, Multiple Equilibria and Propagating Planetary Waves in Baroclinic, Orographically Forced, Planetary Wave Systems. *J. Atmos. Sci.*, **37**, 1157–1176.

- Cheng, X., and J. M. Wallace, 1993: Multiple Flow Equilibria in the Atmosphere Wintertime 500 hPa Height Field: Spatial Patterns. *J. Atmos. Sci.*, **50**, 2674–2696.
- Christiansen, B., 2005: Bimodality of the Planetary-Scale Atmospheric Wave Amplitude Index. *J. Atmos. Sci.*, **62**, 2528–2541.
- Corti, S., F. Molteni, and T. N. Palmer, 1999: Signature of recent Climate Change in Frequencies of Natural Atmospheric Circulation Regimes. *Nature*, **398**, 799–802.
- Crommelin, D. T., 2004: Observed Nondiffusive Dynamics in Large-Scale Atmospheric Flow. *J. Atmos. Sci.*, **61**, 2384–2396.
- D’Andrea, F., S. Tibaldi, M. Blackburn, G. Boer, M. Déqué, M. R. Dix, B. Dugas, L. Ferranti, T. Iwasaki, A. Kitoh, V. Pope, D. Randall, E. Roeckner, D. Straus, W. Stern, H. Van den Dool and D. Williamson, 1998: Northern Hemisphere atmospheric blocking as simulated by 15 atmospheric general circulation models in the period 1979-1988. *Clim. Dyn.*, **14**, 385–407.
- Deloncle, A., R. Berk, F. D’Andrea and M. Ghil, 2007: Weather Regime Prediction Using Statistical Learning. *J. Atmos. Sci.*, **64**, 1620–1635.
- Franzke, C., and A. J. Majda, 2006: Low-order Stochastic Mode Reduction for a Prototype Atmospheric GCM. *J. Atmos. Sci.*, **63**, 457-479.
- Franzke, C., A. J. Majda and G. Branstator, 2007: The Origin of Nonlinear Signatures of Planetary Wave Dynamics: Mean Phase Space Tendencies and Contributions from Non-Gaussianity. *J. Atmos. Sci.*, **64**, 3987-4003.

- Franzke, C., A. J. Majda, and E. Vanden-Eijnden, 2005: Low-order stochastic mode reduction for a realistic barotropic model climate. *J. Atmos. Sci.*, **62**, 1722–1745.
- Franzke, C., D. T. Crommelin, A. Fischer and A. J. Majda, 2008: A Hidden Markov Model Perspective on Regimes and Metastability in Atmospheric Flows. *J. Climate*, **21**, 1740–1757.
- Grote, M. J., A. J. Majda and C. Crotta Ragazzo, 1999: Dynamic Mean Flow and Small-Scale Interaction through Topographic Stress. *J. Nonlinear Sci.*, **9**, 89–130.
- Hansen, A. R. and A. Sutera, 1986: On the Probability Density Distribution of Planetary-Scale Atmospheric Wave Amplitude. *J. Atmos. Sci.*, **43**, 3250–3265.
- Horenko, I., 2008a: Finite element approach to clustering of multidimensional time series. *SIAM J. Sci. Comp.*, , submitted.
- Horenko, I., 2008b: On simultaneous dimension reduction and hidden phase identification. *J. Atmos. Sci.*, **65**, 1941–1954.
- Horenko, I., 2008c: On Clustering of Non-Stationary Meteorological Time Series. *Dyn. of Atmos. and Ocean* , , submitted.
- Horenko, I., 2008d: On robust estimation of low-frequency variability trends in discrete Markovian sequences of atmospherical circulation patterns. *J. Atmos. Sci.*, , accepted for publication.
- Horenko, I., S. Dolaptchiev, A. Eliseev, I. Mokhov and R. Klein, 2008a: Metastable decomposition of high-dimensional meteorological data with gaps. *J. Atmos. Sci.*, **65**, 3479–3496.

- Horenko, I., R. Klein, S. Dolaptchiev, and C. Schütte, 2008b: Automatted generation of reduced stochastic weather models. I: Simultaneous dimension and model reduction for time series analysis. *SIAM Mult. Mod. Sim.*, **6**, 1125–1145.
- Kimoto, K. and M. Ghil, 1993: Multiple Flow Regimes in the Northern Hemisphere Winter. Part I: Methodology and Hemispheric Regimes. *J. Atmos. Sci.*, **50**, 2625–2643.
- Kondrashov, D., J. Shen, R. Berk, F. D’Andrea and M. Ghil, 2008: Predicting Weather Regime Transitions in Northern Hemisphere Datasets. *Clim. Dyn.*, **29**, 535–551.
- Legras, B., and M. Ghil, 1985: Persistent Anomalies, Blocking and Variations in Atmospheric Predictability. *J. Atmos. Sci.*, **42**, 433–471.
- Majda, A. J., C. Franzke and B. Khouider, 2008: An Applied Mathematics Perspective on Stochastic Modelling for Climate. *Phil. Trans. R. Soc. A*, **366**, 2429–2455. doi:10.1098/rsta.2008.0012
- Majda, A. J., I. Timofeyev, and E. Vanden-Eijnden, 1999: Models for stochastic climate prediction. *Proc. Natl. Acad. Sci. USA*, **96**, 14687–14691.
- Majda, A. J., I. Timofeyev, and E. Vanden-Eijnden, 2003: Systematic strategies for stochastic mode reduction in climate. *J. Atmos. Sci.*, **60**, 1705–1722.
- Majda, A. J., C. Franzke, A. Fischer, and D. T. Crommelin, 2006: Distinct Metastable Atmospheric Regimes Despite Nearly Gaussian Statistics: A Paradigm Model. *Proc. Natl. Acad. Sci. USA*, **103**, 8309–8314.
- Metzner, P., I. Horenko and C. Schütte, 2007: Generator Estimation of Markov Jump Processes on Incomplete Observations Non-equisdistant in time. *Phys. Rev. E*, **76**, pp. 066702.

- Michelangeli, P. A., R. Vautard, and B. Legras, 1995: Weather Regimes: Recurrence and quasi stationarity. *J. Atmos. Sci.*, **52**, 1237–1256.
- Mo, K., and M. Ghil, 1988: Cluster Analysis of Multiple Planetary Flow Regimes. *J. Geophys. Res.*, **93**, 10927–10952.
- Monahan, A. H., J. C. Fyfe and G. M. Flato, 2000: A Regime View of Northern Hemisphere Atmospheric Variability and Change Under Global Warming. *Geophys. Res. Lett.* , **27**, 1139–1142.
- Nitsche, G., J. M. Wallace, and C. Kooperberg, 1994: Is there evidence of multiple equilibria in planetary wave amplitude statistics? *J. Atmos. Sci.*, **51**, 314–322.
- Noe, F., 2008: *Probability distributions of molecular observables computed from Markov models. J. of Chem. Phys.*, **128**, 244103.
- Palmer, T. N., F. J. Doblas-Reyes, A. Weisheimer and M. J. Rodwell, 2008: Toward Seamless Prediction: Calibration of Climate Change Projections Using Seasonal Forecasts. *Bull. Amer. Meteorol. Soc.*, doi:10.1175/BAMS-89-4-459
- Pelly, J. L. and B. J. Hoskins, 2003: How well does the ECMWF Ensemble Prediction System predict blocking? *Q. J. R. Meteorol. Soc.*, **129**, 1683–1702.
- Reinhold, B. B., and R. T. Pierrehumbert, 1982: Dynamics of Weather Regimes: Quasi-Steady Waves and Blocking. *Mon. Wea. Rev.*, **110**, 1105–1145.
- Rex, D. F., 1950: Blocking action in the middle troposphere and its effect upon regional climate. *Tellus*, **2**, 196–211.

- Smyth, P., K. Ide, and M. Ghil, 1999: Multiple Regimes in Northern Hemisphere Height Fields via Mixture Modeling Clustering. *J. Atmos. Sci.*, **56**, 3704–3723.
- Stephenson, D. B., A. Hannachi, and A. O’Neill, 2004: On the existence of multiple climate regimes. *Q. J. R. Meteorol. Soc.*, **130**, 583–605.
- Thompson, D. W. J., and J. M. Wallace, 1998: The Arctic Oscillation signature in the wintertime geopotential height and temperature fields. *Geophys. Res. Lett.*, **25**, 1297–1300.
- Tibaldi, S. and F. Molteni, 1990: On the Operational Predictability of Blocking. *Tellus*, **42A**, 343–365.
- Tung, K. K. and A. J. Rosenthal, 1985: Theories of Multiple Equilibria - A Critical Reexamination. Part I: Barotropic Models. *J. Atmos. Sci.*, **42**, 2804–2819.
- Vautard, R., 1990: Multiple Weather Regimes over the North Atlantic: Analysis of Precursors and Successors. *Mon. Wea. Rev.*, **118**, 2056–2081.
- Wiin-Nielsen, A., 1979: Steady States and Stability Properties of a Low-Order Barotropic System with Forcing and Dissipation. *Tellus*, **31**, 375–386.

Figure 1: Eigenvalue spectrum with 95% significance levels according to a probability distribution of Markov Transition matrix fitted to hidden state sequence of topographic stress model and embedding frame = 5. See text for explanation.

Figure 2: Spatial patterns of 500 hPa geopotential height EOF analysis. a) EOF1 (explained variance 11.2%), b) EOF2 (explained variance 7.5%), c) EOF3 (explained variance 6.1%) and d) EOF4 (explained variance 4.9%).

Figure 3: a) Explained variance of 500 hPa geopotential height EOFs, and b) cumulative explained variance of 500 hPa height EOFs.

Figure 4: Eigenvalue spectrum and 95% significance levels according to a probability distribution of Markov Transition matrix fitted to hidden state sequence with frame = 5. See text for explanation.

Figure 5: Hidden state state sequence for representative 500 day sequence.

Figure 6: Conditional mean states of 500 hPa geopotential height composites (left column; Contour interval 100 gpm) and conditional mean states of 500 hPa geopotential height composites with climatological mean subtracted (right column; Contour interval 10 gpm).

Figure 7: a) Projection and b) pattern correlation of Hidden State mean fields onto EOFs.

Figure 8: a) Cumulative histogram of length of hidden state sequences and b) Cumulative histogram of length of hidden state sequences in semi-log display.

Figure 9: Weighted composites according to the left eigenvectors of the Markov transition matrix. Contour interval is 30 gpm.

Figure 10: Conditional transient eddy forcing composites with climatological transient eddy forcing mean subtracted. Left column: full transient eddy forcing (Contour interval $5m^2s^{-2}$), middle column: transient eddy forcing from low-pass filtered anomalies (periods larger than 10 days, contour

interval $5m^2s^{-2}$), right column: transient eddy forcing from high-pass filtered (periods less than 10 days, contour interval $1m^2s^{-2}$) anomalies.

Figure 11: Prediction skill-score.

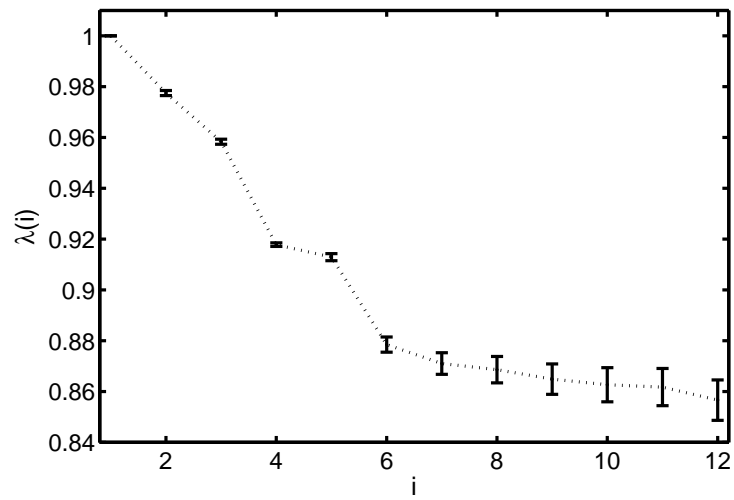
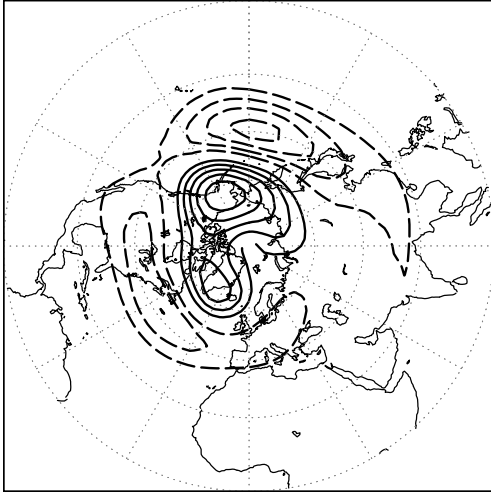
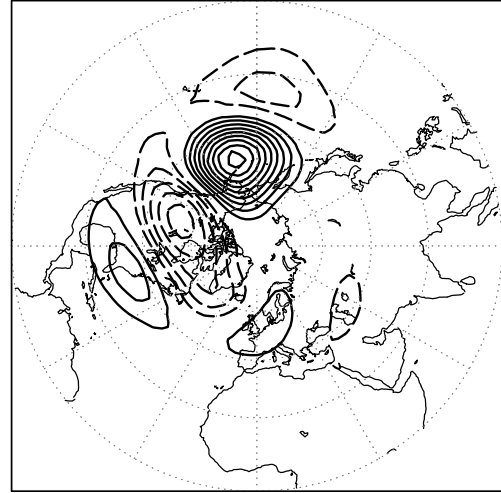


Figure 1: Eigenvalue spectrum with 95% significance levels according to a probability distribution of Markov Transition matrix fitted to hidden state sequence of topographic stress model and embedding frame = 5. See text for explanation.

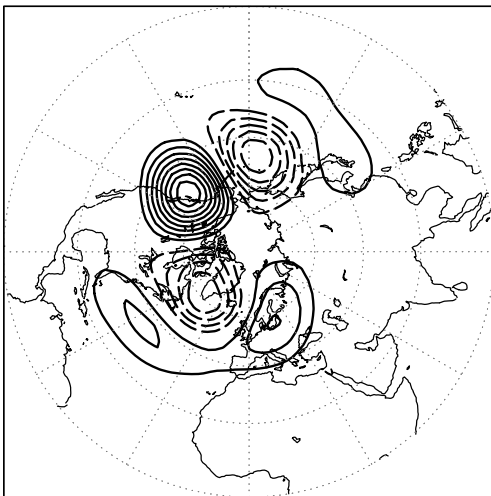
a) EOF1



b) EOF2



c) EOF3



d) EOF4

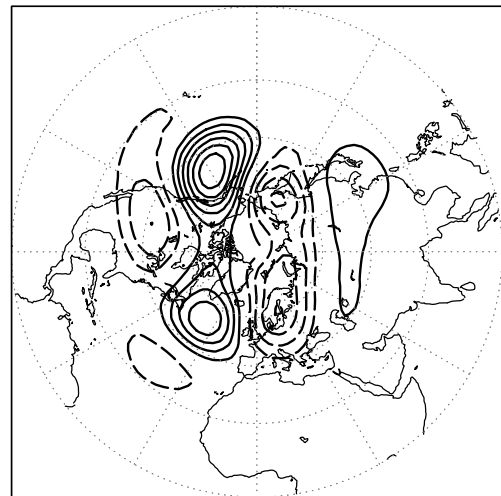


Figure 2: Spatial patterns of 500 hPa geopotential height EOF analysis. a) EOF1 (explained variance 11.2%), b) EOF2 (explained variance 7.5%), c) EOF3 (explained variance 6.1%) and d) EOF4 (explained variance 4.9%).

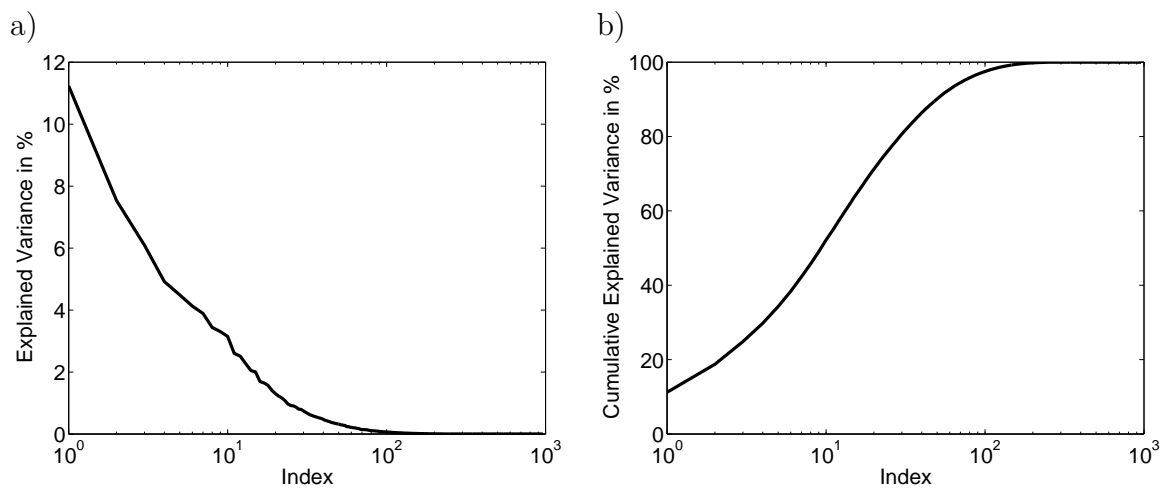


Figure 3: a) Explained variance of 500 hPa geopotential height EOFs, and b) cumulative explained variance of 500 hPa height EOFs.

a)

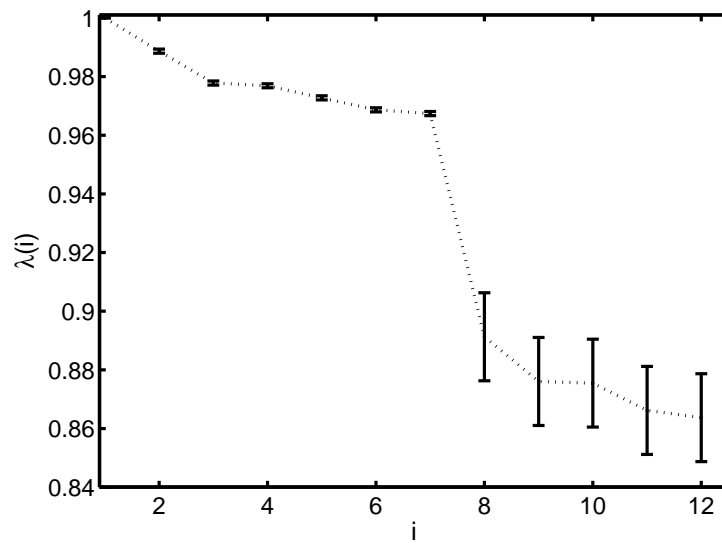


Figure 4: Eigenvalue spectrum and 95% significance levels according to a probability distribution of Markov Transition matrix fitted to hidden state sequence with frame = 5. See text for explanation.

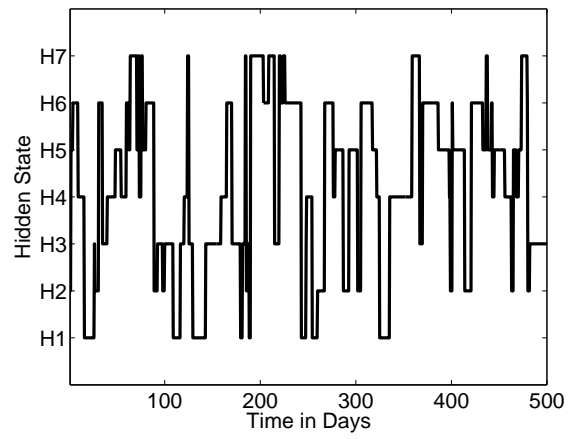
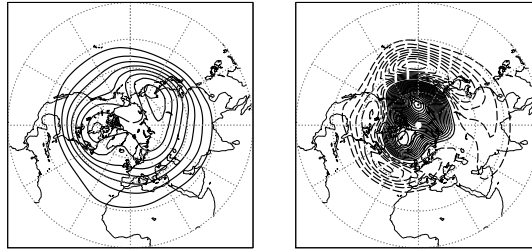
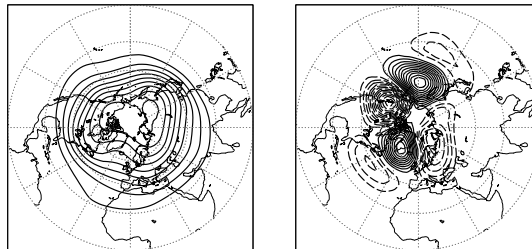


Figure 5: Hidden state state sequence for representative 500 day sequence.

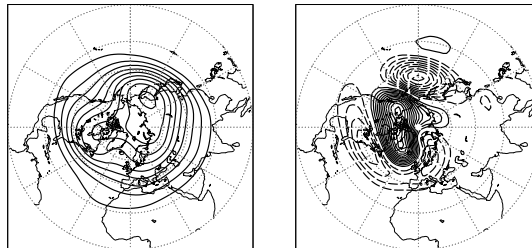
a) Hidden State 1



b) Hidden State 2



c) Hidden State 3



d) Hidden State 4

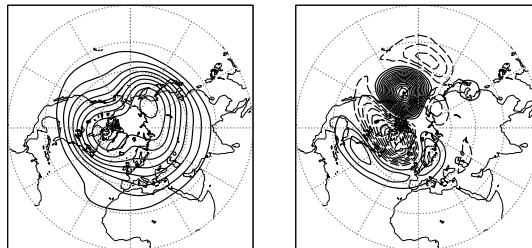
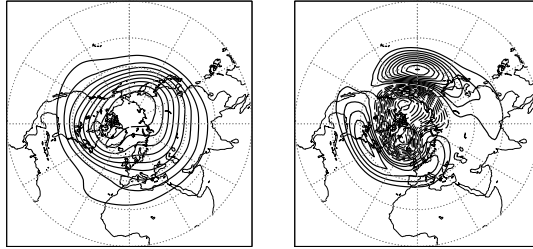
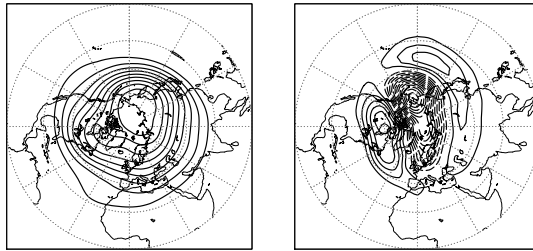


Figure 6: Conditional mean states of 500 hPa geopotential height composites (left column; Contour interval 100 gpm) and conditional mean states of 500 hPa geopotential height composites with climatological mean subtracted (right column; Contour interval 10 gpm).

e) Hidden State 5



f) Hidden State 6



g) Hidden State 7

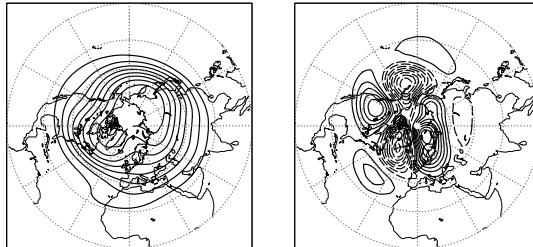
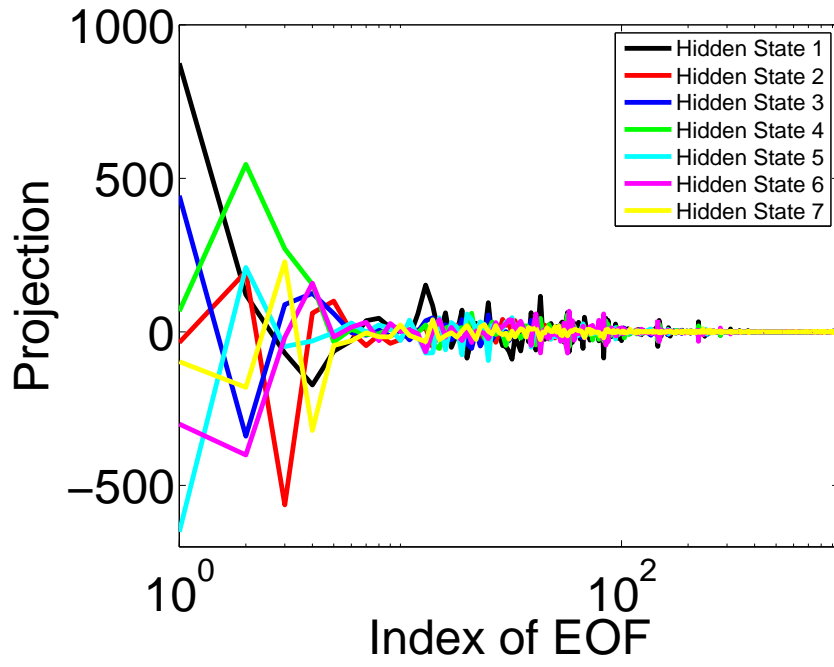


Fig. 6 continued.

a) Projection



b) Correlation

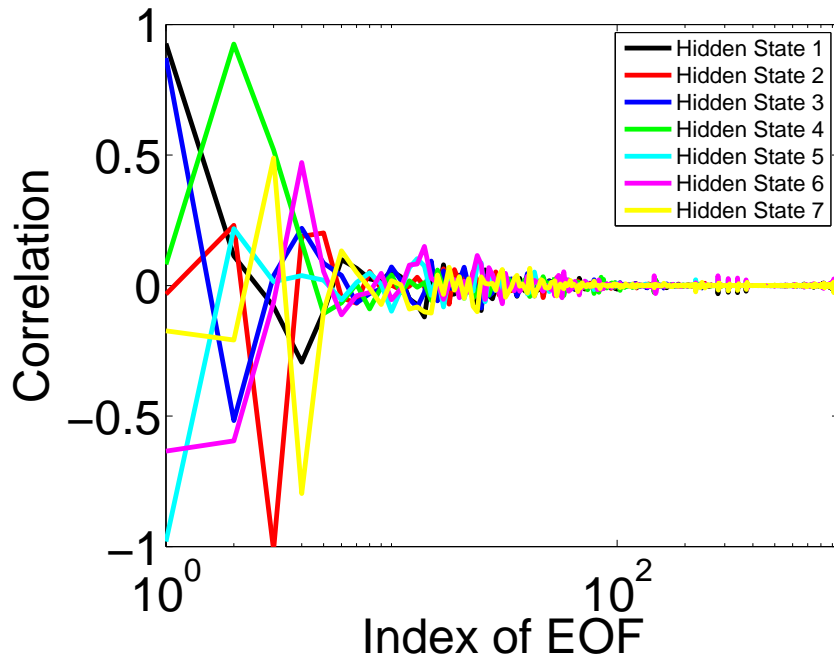


Figure 7: a) Projection and b) pattern correlation of Hidden State mean fields onto EOFs.

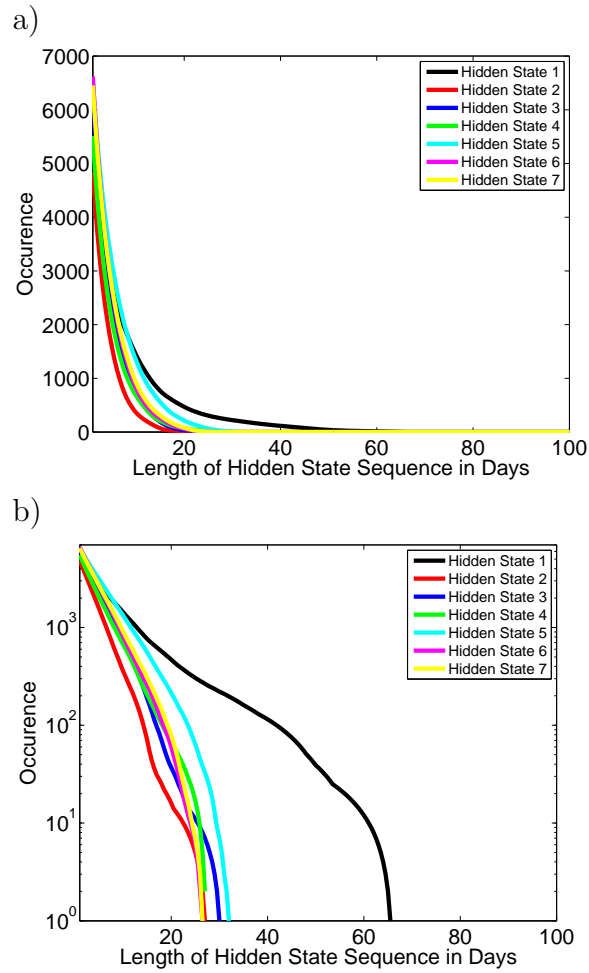
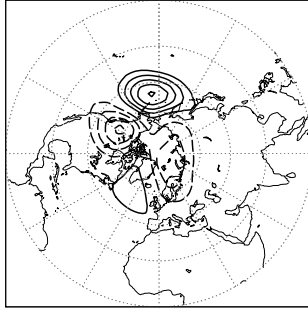
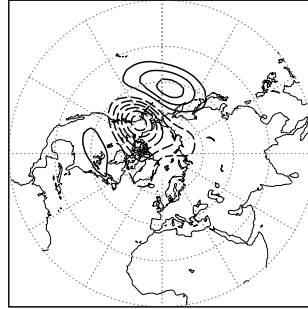


Figure 8: a) Cumulative histogram of length of hidden state sequences and b) Cumulative histogram of length of hidden state sequences in semi-log display.

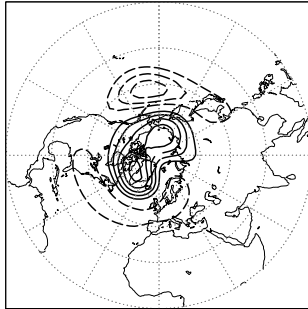
a) Eigenvector 2



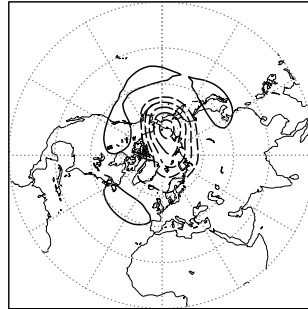
b) Eigenvector 3



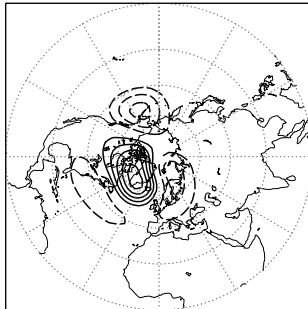
c) Eigenvector 4



d) Eigenvector 5



e) Eigenvector 6



f) Eigenvector 7

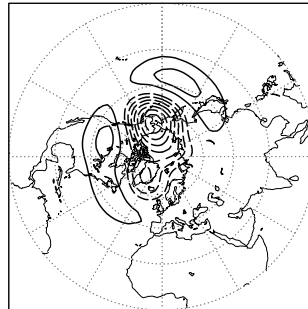


Figure 9: Weighted composites according to the left eigenvectors of the Markov transition matrix. Contour interval is 30 gpm.

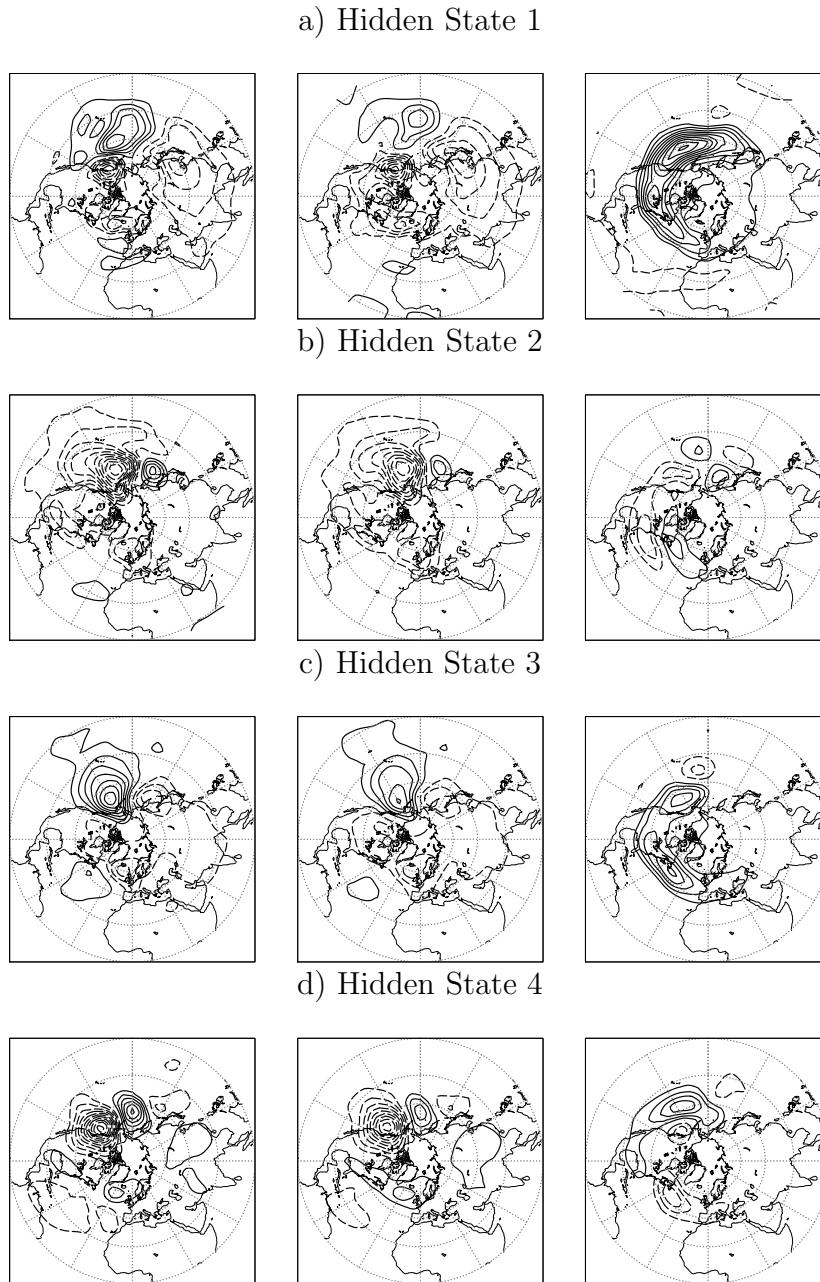
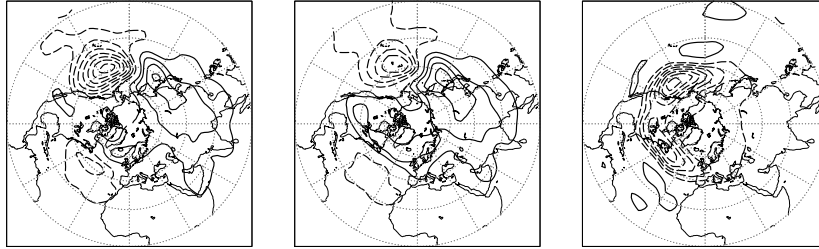
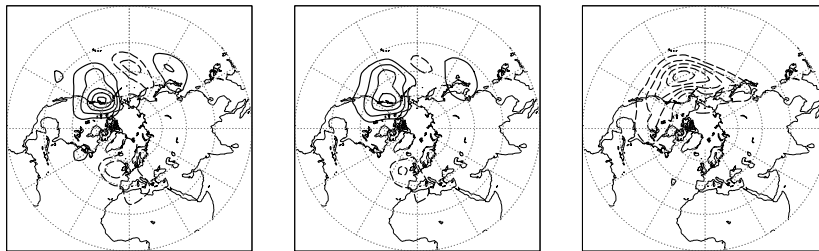


Figure 10: Conditional transient eddy forcing composites with climatological transient eddy forcing mean subtracted. Left column: full transient eddy forcing (Contour interval $5m^2s^{-2}$), middle column: transient eddy forcing from low-pass filtered anomalies (periods larger than 10 days, contour interval $5m^2s^{-2}$), right column: transient eddy forcing from high-pass filtered (periods less than 10 days, contour interval $1m^2s^{-2}$) anomalies.

e) Hidden State 5



f) Hidden State 6



g) Hidden State 7

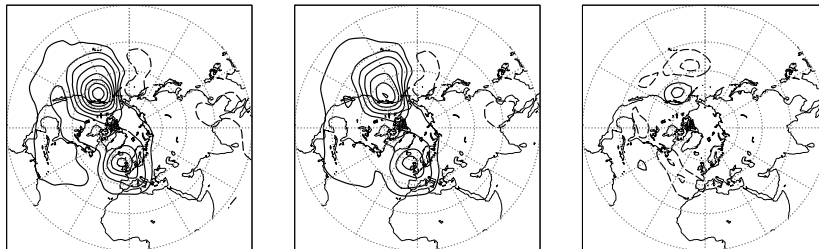


Fig. 10 continued.

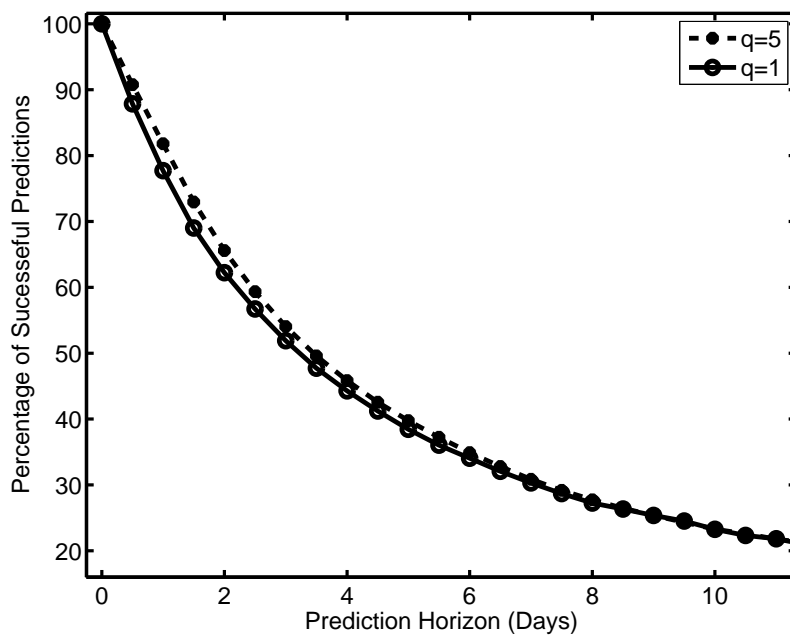


Figure 11: Prediction skill-score.